6 KSME Journal, Vol. 6,No.1, pp. 6~15, 1992

A FINITE ELEMENT PROGRAM FOR SIMULATING SHEET-METAL STRETCH FORMING PROCESSES

Y.T. Keum* and R.H. Wagoner**

(Received June 22, 1991)

A finite-element process modeling program, SHEET-3, was developed using triagnular elements for simulating the sheet-metal stretch forming operation of an arbitrarily-shaped punch and dies. The program employs an implicit, incremental algorithm based on a rigid-viscoplastic constitutive equation with corrections for material unloading. Contact and friction are introduced through a mesh-normal, which compatibly describes arbitrary tool surfaces and FEM meshes without depending on the explicit spatial derivatives of the tool surfaces. The membrane approximation is adopted under the plane-stress assumption. In order to promote convergence, equilibrium and contact iterations are split. For describing an arbitrarily-shaped tool surface, a generalized tool description method is introduced. Simple shape of tools, such as the hemispherical punch and rounded flat-top punch can be analyzed. In addition, any tool described by equally-spaced digital data can be used, based on cubic B-spline or piecewise linear basis functions. The validity, accuracy and stability of the FEM formulation were numerically tested using simple stretch forming examples. Excellent agreement between measured and computed strains was obtained.

Key Words: Sheet-Metal Forming Simulation, Rigid-Viscoplastic Hardening, Press-Die Design Analysis, Membrane Shell Theory, Finite Element Method, Tool Description

NOMENCLATURE

$\Delta\varepsilon_i$: Principal strain increment
$\Delta\bar{\varepsilon}$: Effective strain increment during Δt.
$\Delta\lambda_i$: Principal stretch ratio
Δt : Time increment
$\Delta \boldsymbol{u}$: Incremental displacement during Δt
$\Delta \boldsymbol{u}_t$: Tangential incremental displacement
$\Delta \boldsymbol{u}^*$: Trial incremental displacement
$\delta \boldsymbol{u}$: Correction displacement increment
$\bar{\varepsilon}$: Effective strain
$\dot{\bar{\varepsilon}}$: Effective strain rate
$\boldsymbol{F}_i$: Internal force vector
$\boldsymbol{F}_e$: External force vector
$\boldsymbol{F}_n$: Normal component of $\boldsymbol{F}_e$
$\boldsymbol{F}_t$: Tangential component of $\boldsymbol{F}_e$
$\boldsymbol{\Gamma}$: Contact force direction
$\boldsymbol{K}_e$: External stiffness matrix
$\boldsymbol{K}_i$: Internal stiffness matrix
M : Hill's non-quadratic yield function parameter
m : Strain rate sensitivity index
μ : Coulomb friction coefficient
$\boldsymbol{n}$: Mesh-based normal unit vector
r : Plastic anisotropy parameter
S : Tool surface function, $z=S(x,y)$
σ_i : Principal Cauchy stress
$\bar{\sigma}$: Effective stress
t : Time variable; Length parameter
$\boldsymbol{t}$: Mesh-based tangential unit vector
t_0 : Reference time
V_0 : Volume at $t=t_0$

*CAD/CAM Lab., Korea Institute of Science and Technology, 39-1, Hawolgok-Tong, Sungbuk-Ku, Seoul, 136-191, Korea
**Department of Materials Science and Engineering, The Ohio State University 116 W. 19th Ave., Columbus, OH 43210, U.S.A.

1. INTRODUCTION

A great deal of the time and cost in developing automotive body panels is consumed in design and manufacturing of stamping dies. In general, it is very difficult to predict that a designed part can be stamped successfully. This difficulty is caused by the complex nature of the stamping process. Using the finite element method (FEM), process modeling is capable of predicting the forming loads, overall geometric change of the deforming sheet, distribution of strain and stress, and process condition. According to the simulation results, modifications of tool geometry, material or environmental conditions are implemented for an improved design.

Since Chung and Swift(1951) published analytical and numerical solutions for sheet metal forming processes, many researchers have proposed mathematical models for analyzing sheet forming operations. The first work based on elastic-viscoplastic FEM was done by Wang and Wenner (1978). Later, employing nonlinear membrane theory and incremental plasticity theory, Wang(1982a) developed rigid-plastic FEM. Also using rigid-plastic FEM, Kobayashi and Kim(1978) performed axisymmetric finite-element analysis subject to hydrostatic bulging, punch stretching, and deep-drawing. Oh and Kobayashi (1980) and Toh and Kobayashi (1983) developed finite-element process modeling for general shape forming analyses, and Park et al.(1987), Germain et al. (1989), and Yang et al.(1990) announced rigid-viscoplastic FEM for analyzing simply-shaped punch forming operations. A viscous shell formulation was first introduced by Onate and

Zienkiewicz (1978, 1983). Wood et al.(1978) compared this formulation with others, finding similarities of results. Elastic-viscoplastic FEM formulations for sheet forming analysis have been presented by Wang(1976), Tang(1976), Massoni et al.(1986), and Bellet et al.(1987).

For the spatial and time discretizations in the current formulation, the following assumptions are introduced. First, the rigid-viscoplastic constitutive law, which neglects the elastic strain and involves strain-rate sensitivity, is employed. Since the elastic strain is negligibly small compared to the plastic strain in most stamping processes, only the plastic component is considered. For reflecting the rate sensitivity of forming processes, the hardening law includes strain-rate sensitivity. Second, the membrane approximation is adopted. Zero stress in the orthogonal direction of the local tangent plane is assumed. Because the sheet thickness is relatively small compared to the surface curvature and because in-plahe stretch dominates bending in most stretching operations, this approximation is not unrealistic. Third, a modified Coulomb friction law is implemented to deal with the friction between the sheet and tools. A tangent hyperbolic function is defined in the region of small relative displacement so that the friction force smoothly approaches zero as the relative tangential displacement approaches zero. This friction law approximates the slip-stick condition as an always-slipping one. Fourth, the sheet is assumed to have isotropic properties in the plane and anisotropy in the thickness directions. This normal anisotropy is taken into account through the yield surface with the coefficients of r and M, which is proposed by Hill(1979). Fifth, the yield function isotropically changes during plastic deformation. This isotropic strain hardening plastic flow implies that the yield surface maintains its shape and develops equally in all directions. Sixth, an incremental deformation theory consistent with the time discretization is used in order to overcome the difficulties in the integration of constitutive equations over the time step. This formulation modifies the usual flow theory of plasticity by specifying the plastic path which minimizes the plastic work over the time step (Germain, 1989). By virtue of this path selection, the effective strain increment is uniquely determined by the incremental strains only. So, the stresses become exact function of the incremental displacements (Wang, 1982b). In other words, the incremental displacements uniquely determine the incremental strain and the stress states at the end of the deformation step, independent of path.

The present paper first introduces a mesh-based 3-D FEM program for analyzing sheet metal forming operations. Numerical techniques for improving the convergence and overcoming the numerical difficulties in unloading as well as methods for generating arbitrary tool surfaces are next presented. Finally, the numerical examples illustrate the validity and accuracy of the FEM formulation.

2. THREE-DIMENSIONAL FEM FORMULATION

2.1 Hill's New Yield Theory

For a normal anisotropic material, Hill(1979) introduced a new yield function in order to predict the material behavior under a biaxial state of deformation, i.e., plane stress loading ($\sigma_3=0$). Following Hill's new theory, the effective stress, $\bar{\sigma}$, can be written as follows :

$$\bar{\sigma}=C_1[|\sigma_1+\sigma_2|^M+C_2|\sigma_1-\sigma_2|^M]^{\frac{1}{M}} \tag{1}$$

where $C_1=[2(1+r)]^{\frac{-1}{M}}$ and $C_2=1+2r$.

The principle of normality of yield function (Drucker, 1951), $\dot{\varepsilon}_i=\dot{\lambda}\cdot\frac{\partial f}{\partial\sigma_i}$, yields

$$\dot{\varepsilon}_1=\dot{\lambda}\cdot\{|\sigma_1+\sigma_2|^{M-1}+(1+2r)|\sigma_1-\sigma_2|^{M-1}\} \tag{2}$$
$$\dot{\varepsilon}_2=\dot{\lambda}\cdot\{|\sigma_1+\sigma_2|^{M-1}-(1+2r)|\sigma_1-\sigma_2|^{M-1}\} \tag{3}$$

where $\dot{\varepsilon}_1$ and $\dot{\varepsilon}_2$ are the principal strain rates and $\dot{\lambda}$ is a proportionality constant. Now, the principle of plastic work equivalence says,

$$\bar{\sigma}\cdot\bar{\varepsilon}=\sigma_1\cdot\dot{\varepsilon}_1+\sigma_2\cdot\dot{\varepsilon}_2 \tag{4}$$

where $\dot{\bar{\varepsilon}}$ is the effective strain rate associated with the effective stress, $\bar{\sigma}$. Introducing σ_1 and σ_2 and inverting Eqs. (2) and (3), and $\bar{\sigma}$ in Eq.(1), the effective strain rate in Eq. (4), $\dot{\bar{\varepsilon}}$, can be expressed as follows :

$$\dot{\bar{\varepsilon}}=D_1[|\dot{\varepsilon}_1+\dot{\varepsilon}_2|^{\frac{M}{M-1}}+D_2|\dot{\varepsilon}_1-\dot{\varepsilon}_2|^{\frac{M}{M-1}}]^{\frac{M-1}{M}} \tag{5}$$

where $D_1=\frac{1}{2}[2(1+r)]^{\frac{1}{M}}$ and $D_2=\frac{1}{2}[2(1+r)]^{\frac{-1}{M-1}}$

Hill's new theory defines the shape of the yield surface at every instant during the hardening (Mellor, 1978). The yield surface can change only its size because r and M are constant. Furthermore, σ_i and $\dot{\varepsilon}_i$ in Eqs. (1) and (5) are respectively the eigenvalues of the Cauchy stress tensor and rate-of-deformation tensor.

2.2 Power Law Hardening

The power law is chosen in conjunction with an isotropic hardening rule. The representative stress-strain relationship of this hardening rule, which is determined by experiments, is expressed as follows :

$$\bar{\sigma}=K(\bar{\varepsilon}+\mathrm{a}_o)^n(\dot{\bar{\varepsilon}}/\gamma)^m \tag{6}$$

where $\bar{\sigma}$, $\bar{\varepsilon}(=\int\dot{\bar{\varepsilon}}\,dt)$, K, n and m refer to effective stress, effective strain, strength coefficient, work-hardening exponent, and strain-rate sensitivity index, respectively. γ is a base strain rate and a_o a pre-strain term.

2.3 Finite Element Equilibrium Equation

During the time interval Δt, the plastic work increment, ΔW_p, associated with the minimum energy path can be written as follows :

$$\Delta W_p=\int_{V_o}\left(\int_{t_o}^{t_o+\Delta t}\bar{\sigma}\,\dot{\bar{\varepsilon}}\,dt\right)dV_o$$
$$\int_{V_o}\int_{\bar{\varepsilon}_o}^{\bar{\varepsilon}_o+\Delta\bar{\varepsilon}}\bar{\sigma}(\bar{\varepsilon})\,d\bar{\varepsilon}\,dV_o \tag{7}$$

where $\bar{\varepsilon}_o$ is the effective strain at $t=t_o$ and $\Delta\bar{\varepsilon}$ the amount of increase of effective strain over the time interval Δt :

$$\Delta\bar{\varepsilon}=\int_{t_o}^{t_o+\Delta t}\dot{\bar{\varepsilon}}\,dt \tag{8}$$

Since $\bar{\sigma}(\bar{\varepsilon})$ is always positive in Eq. (7), the minimum energy path also satisfies the minimum of effective strain $\Delta\bar{\varepsilon}$.

Using Eq. (5) and generalizing Damamme's theorem for a tranverse anisotorpic memberane (Damamme, 1978), the minimum of effectve strain increment, $\Delta\bar{\varepsilon}$, defined by Eq. (8) can be written in the following form (Germain, 1989) :

$$\Delta\bar{\varepsilon}=D_1\left[|\ln(\lambda_1\lambda_2)|^{\frac{M}{M-1}}+D_2\left|\ln\left(\frac{\lambda_1}{\lambda_2}\right)\right|^{\frac{M}{M-1}}\right]^{\frac{M-1}{M}} \tag{9}$$

where λ_1 and λ_2 are the principal stretch ratios considered as the eigenvalues of $\sqrt{\boldsymbol{C}}=\boldsymbol{F}^T\boldsymbol{F})^{1/2}$ and $\boldsymbol{F}$ is the deformation gradient between time interval Δt. In Eq. (9), $\Delta\bar{\varepsilon}$ is a function of $\Delta\boldsymbol{u}$ only through λ_1 and λ_2.

The equilibrium equation can be set up by means of the principle of virtual displacements : for every kinematically admissible virtual incremental displacement, $\delta(\Delta\boldsymbol{u})$, during the time interval Δt,

$$\Delta W_{int}=\Delta W_{ext} \tag{10}$$

where ΔW_{int} and ΔW_{ext} are respectively the internal virtual work increment absorbed by the plastic deformation and the external virtual work increment done by the external forces.

Using the plastic work increment, ΔW_p, in Eq. (7), the internal virtual work increment, ΔW_{int}, can be written as follows :

$$\Delta W_{int}=\int_{V_0}\bar{\sigma}\frac{\partial\Delta\bar{\varepsilon}}{\partial\Delta\boldsymbol{u}}\delta(\Delta\boldsymbol{u})\,dV_o \tag{11}$$

The external virtual work increment, ΔW_{ext}, is also defined by the traction caused by tool contact, $\boldsymbol{f}_e$:

$$\Delta W_{ext}=\int_{A_C}\boldsymbol{f}_e\delta(\Delta\boldsymbol{u})\,dA_C \tag{12}$$

where A_C is the contact area at time $t_o+\Delta t$.

By the definition of virtual work principle, Eq. (10), the equilibrium equation is, then, given by :

$$\int_{V_0}\bar{\sigma}\frac{\partial\Delta\bar{\varepsilon}}{\partial\Delta\boldsymbol{u}}\delta(\Delta\boldsymbol{u})\,dV_o=\int_{A_C}\boldsymbol{f}_e\delta(\Delta\boldsymbol{u})\,dA_C \tag{13}$$

for all kinematically admissible $\delta(\Delta\boldsymbol{u})$.

In the finite element method, $\delta(\Delta\boldsymbol{u})$ is the nodal virtual displacement and is not a function of spatial coordinates. So. the equlibrium equation becomes

$$\boldsymbol{F}_i(\Delta\boldsymbol{u})=\boldsymbol{F}_e(\Delta\boldsymbol{u}) \tag{14}$$

where $\boldsymbol{F}_i$ is the internal force derived from the left side of Eq. (13) :

$$\boldsymbol{F}_i=\int_{V_0}\bar{\sigma}\frac{\partial\Delta\bar{\varepsilon}}{\partial\Delta\boldsymbol{u}}\,dV_o, \tag{15}$$

and $\boldsymbol{F}_e$ is the external force derived from the right side of Eq. (13) :

$$\boldsymbol{F}_e=\int_{A_C}\boldsymbol{f}_e\,dA_C \tag{16}$$

Discretizing the whole domain of the sheet workpiece into finite elements, the incremental equilibrium equation, Eq. (14), becomes

$$\boldsymbol{F}_i(\Delta\boldsymbol{u}_k)=\boldsymbol{F}_e(\Delta\boldsymbol{u}_k) \tag{17}$$

where $\Delta\boldsymbol{u}_k$ denotes the incremental displacement of the kth mode, and $\boldsymbol{F}_i(\Delta\boldsymbol{u}_k)$ and $\boldsymbol{F}_e(\Delta\boldsymbol{u}_k)$ are respectively the internal force vector and external contact force vector at node k. Eq. (17) simply means the balance of internal force resisting plastic deformation and the external force caused by the tool contact.

Since $\boldsymbol{F}_i(\Delta\boldsymbol{u})$ can be replaced by $x(\Delta\boldsymbol{u})\cdot\Delta\boldsymbol{u}$ as in static FEM, omitting the node index k, Eq. (17) may be written as :

$$x(\Delta\boldsymbol{u})\cdot\Delta\boldsymbol{u}=\boldsymbol{F}_e(\Delta\boldsymbol{u}) \tag{18}$$

Eq. (18) can be solved by the Newton-Raphson method. For this method, Eq. (18) is expanded in a Taylor series about a trial solution $\Delta\boldsymbol{u}^*$, i.e.

$$\Delta\boldsymbol{u}=\Delta\boldsymbol{u}^*+\delta\boldsymbol{u} \tag{19}$$

and only first order terms are retained :

$$\left(\frac{\partial\boldsymbol{F}_i}{\partial\Delta\boldsymbol{u}}-\frac{\partial\boldsymbol{F}_e}{\partial\Delta\boldsymbol{u}}\right)\Big|_{\Delta\boldsymbol{u}}\delta\boldsymbol{u}=\boldsymbol{F}_e(\Delta\boldsymbol{u}^*)-\boldsymbol{F}_i(\Delta\boldsymbol{u}^*) \tag{20}$$

A simple change of notation allows Eq. (20) into

$$\boldsymbol{K}\cdot\delta\boldsymbol{u}=\boldsymbol{F}_e-\boldsymbol{F}_i \tag{21}$$

where $\boldsymbol{K}$ is the tangent stiffness matrix at the trial increment displacement, $\Delta\boldsymbol{u}^*$, expressed by

$$\boldsymbol{K}=\boldsymbol{K}_i-\boldsymbol{K}_e=\left(\frac{\partial\boldsymbol{F}_i}{\partial\Delta\boldsymbol{u}}-\frac{\partial\boldsymbol{F}_e}{\partial\Delta\boldsymbol{u}}\right)\Big|_{\Delta\boldsymbol{u}^*}, \tag{22}$$

and $\delta\boldsymbol{u}$ is an incremental correction displacement vector which is zero at equilibrium. Letting h_o be the original sheet thickness and considering $dV_o=h_o\cdot dA_o$, $\boldsymbol{F}_i$ (the internal force at $\Delta\boldsymbol{u}^*$) is defined by Eq. (15):

$$\boldsymbol{F}_i=\boldsymbol{h}_o\int_{A_o}\bar{\sigma}\frac{\partial\Delta\bar{\varepsilon}}{\partial\Delta\boldsymbol{u}}\Big|_{\Delta\boldsymbol{u}=\Delta\boldsymbol{u}^*}dA_o \tag{23}$$

and $\boldsymbol{F}_e$ is the external force. $\boldsymbol{F}_e-\boldsymbol{F}_i$ is the residual force vector for a trial solution, $\Delta\boldsymbol{u}^*$. Explicitly, the terms of Eq. (22) may be found to be as follows :

$$\boldsymbol{K}_i=\frac{\partial\boldsymbol{F}_i}{\partial\Delta\boldsymbol{u}}\Big|_{\Delta\boldsymbol{u}^*}=h_o\int_{A_o}\left\{\bar{\sigma}(\bar{\varepsilon}+\Delta\bar{\varepsilon},\dot{\bar{\varepsilon}})\frac{\partial^2\Delta\bar{\varepsilon}}{\partial\Delta u\,\partial\Delta\boldsymbol{u}}+\left(\frac{\partial\bar{\sigma}}{\partial\bar{\varepsilon}}+\frac{1}{\Delta t}\frac{\partial\bar{\sigma}}{\partial\dot{\bar{\varepsilon}}}\right)\frac{\partial\Delta\bar{\varepsilon}}{\partial\Delta\boldsymbol{u}}\frac{\partial\Delta\bar{\varepsilon}}{\partial\Delta\boldsymbol{u}}\right\}\Big|_{\Delta\boldsymbol{u}=\Delta\boldsymbol{u}^*}dA_o \tag{24}$$

$$\boldsymbol{K}_e=\frac{\partial\boldsymbol{F}_e}{\partial\Delta\boldsymbol{u}}\Big|_{\Delta\boldsymbol{u}=\Delta\boldsymbol{u}^*} \tag{25}$$

In Eqs. (23) and (24), $\frac{\partial\Delta\bar{\varepsilon}}{\partial\Delta\boldsymbol{u}}$ and $\frac{\partial^2\Delta\bar{\varepsilon}}{\partial\Delta\boldsymbol{u}\,\partial\Delta\boldsymbol{u}}$ for a finite element can be derived using Eq. (9) [Wang(1984), Germain(1989), Keum(1990b)]. Furthermore, $\bar{\sigma}$, $\frac{\partial\bar{\sigma}}{\partial\bar{\varepsilon}}$ and $\frac{\partial\bar{\sigma}}{\partial\dot{\bar{\varepsilon}}}$ ae calculated using Hill's new yield criterion and flow rule, and power law hardening at the trial solution, $\Delta\boldsymbol{u}^*$. Therefore, $\boldsymbol{F}_i$ and $\boldsymbol{K}_i$ of Eqs. (23) and (24) can be numerically evaluated.

Where the sheet is in contact with the tools, the external force, $\boldsymbol{F}_e$, is given by the Coulomb friction law for slipping conditions:

$$\boldsymbol{F}_e = F_n(\mu \boldsymbol{t} + \boldsymbol{n}), \tag{26}$$

where $\boldsymbol{F}_n$ and μ are the resultant normal force magnitude at the contact node and coefficient of friction. In Eq. (26), $\boldsymbol{n}$ is a unit nodal normal vector outward to the tool (usual formulation) or mesh (present formulation) at each contacting node and $\boldsymbol{t}$ is a tangential vector oppositely parallel to the motion of each contacting node during the time increment defined by:

$$\boldsymbol{t} = -\frac{\boldsymbol{n}\times\Delta\boldsymbol{u}\times\boldsymbol{n}}{\|\boldsymbol{n}\times\Delta\boldsymbol{u}\times\boldsymbol{n}\|} \tag{27}$$

The slip-stick Coulomb condition is modified by introducing ϕ, a prescribed function of the sliding incremental displacement magnitude relative to the tangential incremental displacement magnitude, $\|\Delta\boldsymbol{u}_t\|$. ϕ is a smoothing factor such that the friction force smoothly approaches zero as the tangential displacement approaches zero. For large tangential displacements, ϕ goes to 1. In this formulation, hyperbolic tangent function (tanh) is employed for the smooth function [Keum(1990b)].

Using the smoothing function ϕ, Eq. (26) may be written as follows:

$$\boldsymbol{F}_e = (\mu\phi(\Delta\boldsymbol{u}_t)\,\boldsymbol{t} + \boldsymbol{n})\,F_n \tag{28}$$

Therefore, the external stiffness matrix, $\boldsymbol{K}_e$ in Eq. (25), becomes

$$\begin{aligned}\boldsymbol{K}_e &= \frac{\partial \boldsymbol{F}_e}{\partial \Delta\boldsymbol{u}}\Big|_{\Delta u^*} \\ &= \left(\mu\left(\frac{\partial\phi(\Delta\boldsymbol{u}_t)}{\partial\Delta\boldsymbol{u}}\right)\boldsymbol{t} + \phi(\Delta\boldsymbol{u}_t)\frac{\partial\boldsymbol{t}}{\partial\Delta\boldsymbol{u}} + \frac{\partial\boldsymbol{n}}{\partial\Delta\boldsymbol{u}}\boldsymbol{F}_n\right)\Big|_{\Delta u^*} \\ &\quad + (\mu\phi(\Delta\boldsymbol{u}_t)\,\boldsymbol{t} + \boldsymbol{n})\frac{\partial F_n}{\partial\Delta\boldsymbol{u}}\Big|_{\Delta u^*}\end{aligned} \tag{29}$$

where $\frac{\partial F_n}{\partial\Delta\boldsymbol{u}}$ is defined at the trial solution as follows:

$$\frac{\partial F_n}{\partial\Delta\boldsymbol{u}} = \frac{\partial}{\partial\Delta\boldsymbol{u}}(\boldsymbol{F}_i\cdot\boldsymbol{n}) = \boldsymbol{K}_i\cdot\boldsymbol{n} + \boldsymbol{F}_i\cdot\frac{\partial\boldsymbol{n}}{\partial\Delta\boldsymbol{u}} \tag{30}$$

In Eqs. (28) and (29), $\boldsymbol{F}_e$ and $\boldsymbol{K}_e$ are functions of $\Delta\boldsymbol{u}$, $\boldsymbol{n}$, $\boldsymbol{t}$, $\frac{\partial\boldsymbol{n}}{\partial\Delta\boldsymbol{u}}$, and $\frac{\partial\boldsymbol{t}}{\partial\Delta\boldsymbol{u}}$.

2.4 Normal Vector and Tangential Vector

Figure 1 shows the mesh-normal vector defined by the connected elements at a node. Each connected element has an element normal vector($\boldsymbol{N}_k$) represented at the geometric center. Considering these element normal vectors, the node normal vector, $\boldsymbol{n}$, at the contact node j is evaluated by a weighted average of connected element normals as foloows:

$$\boldsymbol{n} = \frac{\sum_{k=1}^{n_e}\theta_k\boldsymbol{N}_k}{\|\sum_{k=1}^{n_e}\theta_k\boldsymbol{N}_k\|}, \tag{31}$$

where $\boldsymbol{n}_e$ is the number of elements containing node j, θ_k is the included angle of element k at node j(Fig. 1), and $\boldsymbol{N}_k$ is the normal to the k—th element connected to node j. Using two line vectors lying on the k—th element, dx_1 and dx_2, i.e.

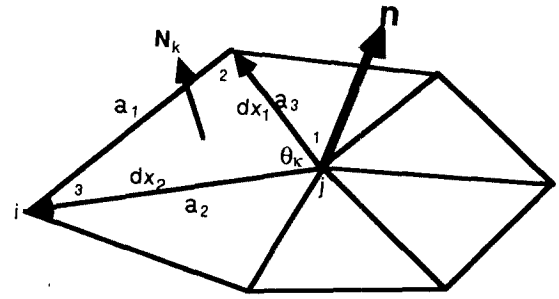

Fig. 1 Definition of mesh-normal vector from connected finite elements

$$\boldsymbol{N}_k = \frac{dx_1\times dx_2}{\|dx_1\times dx_2\|} \tag{32}$$

$$\theta_k = \cos^{-1}\left(\frac{dx_1\cdot dx_2}{\|dx_1\|\|dx_2\|}\right) \tag{33}$$

the pertinent quantities may be found. By rewriting the element normal unit vector, $\boldsymbol{N}_k$, in the following component form:

$$\boldsymbol{N}_k = (N_{xk},\ N_{yk},\ N_{zk}), \tag{34}$$

the components of $\boldsymbol{N}_k$ can be computed from Eq. (32) as follows:

$$N_{xk} = \frac{C_1}{C};\ N_{yk} = \frac{C_2}{C};\ N_{zk} = \frac{C_3}{C} \tag{35}$$

where
$$\begin{aligned} C_1 &= (y_2-y_1)(z_3-z_1) - (z_2-z_1)(y_3-y_1) \\ C_2 &= (z_2-z_1)(x_3-x_1) - (x_2-x_1)(z_3-z_1) \\ C_3 &= (x_2-x_1)(y_3-y_1) - (y_2-y_1)(x_3-x_1) \\ C &= \sqrt{C_1^2+C_2^2+C_3^2}\end{aligned} \tag{36}$$

In Eq. (36), x_i, y_i and z_i are the spatial coordinates of the i—th node position in element k and subscript numbers are nodal sequences for element k in Fig. 1.

If a_1, a_2 and a_3 are respectively edge lengths of element k associated with nodal sequence numbers, 1, 2 and 3, then the included angle, θ_k, can be expressed as follows:

$$\theta_k = \cos^{-1}\left(\frac{a_2^2+a_3^2-a_1^2}{2a_2a_3}\right) \tag{37}$$

where
$$\begin{aligned} a_1^2 &= (x_3-x_2)^2+(y_3-y_2)^2+(z_3-z_2)^2 \\ a_2^2 &= (x_3-x_1)^2+(y_3-y_1)^2+(z_3-z_1)^2 \\ a_3^2 &= (x_2-x_1)^2+(y_2-y_1)^2+(z_2-z_1)^2\end{aligned} \tag{38}$$

So, after calculating the connective element normal, $\boldsymbol{N}_k$, by Eqs. (34) and (35), and the included angle, θ_k, by Eq. (37) for every element containing the jth node, the global normal unit vector at the contact node, $\boldsymbol{n}$, is calculated from Eq. (31) by the usual assembly procedure.

After finding the global normal unit vector, $\boldsymbol{n}$, from Eq. (31), the tangential unit vector, $\boldsymbol{t}$, which has a direction normal to the mesh normal vector and which is oriented in that normal plane opposite to the projection of the nodal

displacement, $\Delta \boldsymbol{u}$, onto that plane, can be found using Eq. (27).

Employing the normal and tangential vectors in Eq. (31) and Eq. (27), the derivatives with respect to the nodal incremental displacement vector, $\frac{\partial \boldsymbol{n}}{\partial \Delta \boldsymbol{u}}$ and $\frac{\partial \boldsymbol{n}}{\partial \Delta \boldsymbol{u}'}$ can be obtained from the connectivity. (Keum, 1990 a and 1990b)

The normal and tangential vectors, and their spatial derivatives are related to the neighboring nodes associated with that node. In other words, the surface normals, tangents, and their derivatives at each FEM node are evaluated directly from the FEM mesh.

3. NUMERICAL IMPLEMENTATION

3.1 Contact Constraint

In order to solve Eq. (21) for $\delta \boldsymbol{u}$, it is necessary to specify $\boldsymbol{F}_e$ on a node—by—node basis depending on whether the node has already been in contact with the tool or not. For a node in contact with the punch, a constraint equation for $\delta \boldsymbol{u}$ which forces the node to lie on the punch and to move in the tangent plane must be satisfied. Furthermore, $\boldsymbol{F}_e$(given by Eq. (28)) is specified for a slipping node subject to coublomb friction.

A node located on the punch surface at time $t+\Delta t$, is constrained to move in the tangent plane, a point defined by the trial solution, $\Delta \boldsymbol{u}^*$. The tangent plane incorporates the first derivatives at a contact point, $\overline{ZX}$ and $\overline{ZY}$. The constraint on $\delta \boldsymbol{u}=(\delta u_x, \delta u_y, \delta u_z)$, for contacting nodes is then:

$$\delta u_z = \overline{ZX} \cdot \delta u_x + \overline{ZY} \cdot \delta u_y \tag{39}$$

In the tool-normal formulation, $\overline{ZX}$ and $\overline{ZY}$ in Eq. (39) are respectively replaced by the spatial derivatives of tool surface, S_x and S_y.

For a slipping node, the unknowns are the components of the correction vector $\delta \boldsymbol{u}=(\delta u_x, \delta u_y, \delta u_z)$ and the normal contact force F_n. There are four equations available: 3 equations by Eq. (21), and 1 equation of constraint, Eq. (39). Since F_n appears in the coefficients of Eq. (21), only iterative methods can be used to get the exact value of F_n.

In order to simplify this process, we estimate the value of F_n so that there is only $\delta \boldsymbol{u}$ left unknown. F_n is chosen equal to:

$$F_n = \boldsymbol{F}_i(\Delta \boldsymbol{u}^*) \cdot \boldsymbol{n}, \tag{40}$$

where $\boldsymbol{F}_i(\Delta \boldsymbol{u}^*)$ is given by Eq. (23). This value is a good estimate of the real F_n because Eq. (40) is satisfied when the trial solution converges. Now, only $(\delta u_x, \delta u_y, \delta u_z)$ remains to be solved.

The last step is the substitution of lines in the linear system in order to include the constraint condition, Eq. (39). Let the three lines corresponding to the contact node be labeled (1), (2) and (3) in the linear system of equilibrium equations, Eq. (21), and let the direction of the total contact force operating at the node be $\boldsymbol{\Gamma}(=\boldsymbol{n}+\mu \cdot \boldsymbol{t})$, then the contact force, $\boldsymbol{F}_e$, in terms of F_n and $\boldsymbol{\Gamma}$ is expressed as follows:

$$\boldsymbol{F}_e = F_n \boldsymbol{\Gamma} = F_n(\mu \boldsymbol{t} + \boldsymbol{n}) \tag{41}$$

If the components of the contact force direction vector, $\boldsymbol{\Gamma}$, are denoted $(\Gamma_1, \Gamma_2, \Gamma_3)$, the system of equilibrium equations at contact nodes is defined by the following procedures: With $\boldsymbol{a}$, a vector perpendicular to $\boldsymbol{\Gamma}$, the contact condition requires that

$$\boldsymbol{F}_i \cdot \boldsymbol{a} = 0. \tag{42}$$

By the definition of $\boldsymbol{a}$, $\boldsymbol{\Gamma} \cdot \boldsymbol{a}=0$ and a can be defined, in terms of $\boldsymbol{\Gamma}$ components, by

$$\boldsymbol{a} = x[1, 0, -\Gamma_1/\Gamma_3]^T + y[0, 1, -\Gamma_2/\Gamma_3]^T \tag{43}$$

for every possible x and y. Noting that $\boldsymbol{F}_i=[F_x, F_y, F_z]^T$, two independent equations can be derived from Eqs. (42) and (43), i.e.

$$\begin{aligned} \Gamma_3 \cdot F_x - \Gamma_1 \cdot F_z &= 0 \\ \Gamma_3 \cdot F_x - \Gamma_2 \cdot F_z &= 0 \end{aligned} \tag{44}$$

Since F_x, F_y and F_z are respectively expressed as (1), (2) and (3) in the force vector of the contacting node, Eq. (44) may be rewritten as follows:

$$\begin{aligned} &(1) \text{ becomes } \Gamma_3 \cdot (1) - \Gamma_1 \cdot (3) \\ &(2) \text{ becomes } \Gamma_3 \cdot (2) - \Gamma_2 \cdot (3) \end{aligned} \tag{45}$$

Therefore, Eqs. (39) and (45) represent contact conditions.

3.2 Unloading Scheme

The rigid-viscoplastic constitutive equation can be applied

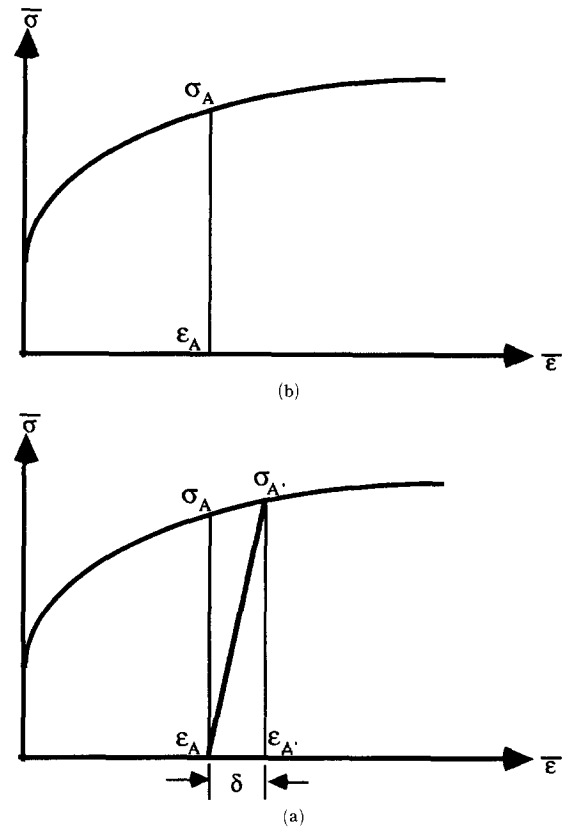

Fig. 2 (a) Hardening curve and (b) Modification to deal with material unloading quasi-elastically

only to the elements which plastically deform. The effective stress, $\bar{\sigma}$, is a function of the total effective plastic strain, $\bar{\varepsilon}$, following the hardening curve. It can happen that the stress balace in the material requires the effective strain increment to vanish. The element tends to unload and the equilibrium condition, Eq. (14), cannot be satisfied. This problem is a limitation of the rigid-viscoplastic approach. For a rate-insensitive material, during the deformation (positive plastic loading), the stress state stays on the solid line of Fig. 2(a). When the unloading happens at ε_A, the strain state is frozen and the stress state is on the line below σ_A. If the material is rate-sensitive, the material element can be unloaded by decreasing the deforming rate. The more the material is rate-sensitive, the more unloading ability the material has without resorting to the quasi-elastic unloading scheme. Calculations for metals having low rate-sensitivity, therefore, have a non-equilibrium problem.

Besides the unloading situation, the problem of indeterminancy also occurs if the hardening law has a non-zero, finite stress at zero strain. In this case, a solution cannot be available until the load becomes large enough to deform fully.

In order to cope with this indeterminacy problem, the following quasi-linear approaches are pursued. When a steep linear hardening line is introduced between ε_A and σ_A, as seen in Fig. 2(b), the hardening law for each step consists of two parts; If $\Delta\bar{\varepsilon}$ is smaller than δ, a linear hardening law is used and if $\Delta\bar{\varepsilon}$ is bigger than δ, the nonlinear hardening curve is employed. Note that the linear relation newly introduced is a change only in the hardening relation, still keeping the incremental deformation plasticity law. (Hence, the assumed response is quasi-elastic.)

3.3 Trial Solution, Update and Convergence

In order to improve convergence, a split-iteration algorithm has been introduced. For each trial set of contacting and noncontacting nodes, an equilibrium iteration is performed without updating contact status, until equilibrium is satisfied. After equilibrium is satisfied (for the specified node contact condition), the nodes are reexamined for consistency (i.e. compressive normal force) and penetration. The contact set is then updated by releasing or projecting certain nodes and another equilibrium iteration is initiated. The non-penetration contact condition is applied by projecting interior nodes to the surface along a specified path, either the minimum distance, the z-direction, or along the mesh-normal vector. A fractional norm of difference in displacements between the given trial and the modified trial is calculated. When this norm is small enough, the current contact iteration becomes final.

The solution of the equilibrium equation, by the Newton-Raphson method, provides the correction vector for the next set of trial displacements. Whithin this equilibrium iteration, the internal force and its corresponding stiffness are calculated. The contact force and stiffness are next computed for the equilibrium equation, based on the unchanged contact and friction condition. These displacements are updated purely by Newton-Raphson updates, without updating the contact status of each node. To determine the convergence in equilibrium, a fractional norm of the correction displacements to the incremental displacements, N_f, is evaluated:

$$N_f=\frac{\|\delta \boldsymbol{u}\|}{\|\Delta \boldsymbol{u}^*\|} \tag{46}$$

where $\|\cdot\|$ denotes the cartesian norm of the nodal vector. When this criterion falls below a specified value, usually 10^{-5}, convergence is declared. Once convergence is obtained, the nodes having a non-compressive force are released. If the current contact iteration is already set final, the punch displacement is incremented for another time step. Otherwise, another contact iteration is repeated.

If Δt_1 and Δt_2 denote the magnitudes of the previous and current time steps, respectively, the trial solution is simply taken equal to:

$$\Delta \boldsymbol{u}^*=\Delta \boldsymbol{u}^{(old)}\cdot\frac{\Delta t_2}{\Delta t_1} \tag{47}$$

When the equilibrium iteration is converged inside the final contact iteration, the norm of residual force becomes less than 10^{-3}. The trial solution is updated by adding the correction vector $\delta \boldsymbol{u}$. Whenever the trial solution is not in a close neighborhood of the actual solution, numerical results show that the convergence is very difficult to achieve. An attempt to reduce this difficulty is made by using the following update scheme: with $0<\beta\leq 1$,

$$\Delta \boldsymbol{u}^{*(new)}=\Delta \boldsymbol{u}^{*(old)}+\beta\cdot\delta \boldsymbol{u} \tag{48}$$

where β is first taken equal to a value of function of N_f, which is suggested by Wang(1982a, 1984). β is then divided by 2 until the residual force norm starts to decrease. The time step is automatically divided in half if no β-values are found after 7 divisions. The iterations of Newton-Raphson are then started again with the trial solutions scaled according to the new time step.

When the displacement correction norm and the contact conditional norm fall below a specified value, convergence is declared and the punch displacement is incremented for another time step.

3.4 Projection Scheme

Duirng equilibrium iteration, a nodal position updated by Newton-Raphson may penetrate the punch or die. If so, the nodal coordinates are modified (in the contact iteration) by a projection scheme such that the node just touches the punch or die surface. Currently, z-direction projection, minimum distance projection, and mesh-normal direction projection are available.

(1) Z-Direction Projection: Only the z coordinate is modified so that the node just comes into contact with the surface of the punch or die. Numerical results have shown that this method destabilizes the convergence of the Newton-Raphson method as soon as the derivatives of the tool surface with respect to z are not small. This method is efficient in computation time since the punch surface is easily found at any given x and y.

(2) Tool-Normal Projection: The new location of the penetrated node is the point of the surface of the punch (or die) defined by the shortest distance between the trial nodal position and the surface. The new location (x, y, z) is related to the trial coordinates (X, Y, Z) by:

$$\underset{x,y,z}{\mathrm{MIN}}\{(x-X)^2+(y-Y)^2+(z-Z)^2\} \text{ in } z=S(x,y) \tag{49}$$

where S is the surface equation of the punch or die at time t.

This equation is nonlinear and is solved by the Newton-Raphson method.

(3) Mesh-Normal Projection: The position of a penetrated node is modified to locate it at the tool surface where the mesh-normal vector for that node intersects it. After calculating the mesh-normal vector, $\boldsymbol{n}(n_x, n_y, n_z)$, for the current mesh geometry, the tool surface point to be projeced, $(\boldsymbol{t}\cdot\boldsymbol{n}_x,\ \boldsymbol{t}\cdot\boldsymbol{n}_y,\ \boldsymbol{t}\cdot\boldsymbol{n}_z)$, can be iteratively found by solving for the length parameter, t, for the nonlinear equation:

$$S(\boldsymbol{t}\cdot\boldsymbol{n}_x,\ \boldsymbol{t}\cdot\boldsymbol{n}_y)-\boldsymbol{t}\cdot\boldsymbol{n}_z=0 \tag{50}$$

where $S(x,\ y)$ is the tool surface equation.

3.5 Mechanical Consistency

A nodal point can become free after being in contact. When contact is made, the normal force exerted on the sheet by the rigid punch or die, F_n, can only be compressive by definition: with a normal unit vector, $\boldsymbol{n}$, defined outward to the tool, the normal force can only be non-positive. A tensile force would mean that the punch(or die) surface has properties of sticking the point in the normal direction, a physically unrealistic condition. If the sign of F_n is positive, the node contact status changes from the contacted situation to the free situation.

The normal force, F_n, is calculated from the decomposition of external force:

$$F_n=\boldsymbol{F}_e\cdot\boldsymbol{n} \tag{51}$$

where $\boldsymbol{n}$ is the normal vector at a contact node.

4. PUNCH/DIE SURFACE DESCRIPTION

In order to calculate the normal vector, tangential vector, and the derivatives needed in the Newton-Raphson procedure and in order to apply the non-penetration boundary condition, the mesh-based formulation requires only the z-coordinate from the mathematical description of tool geometry.

For describing an arbitrarily-shaped tool surface, the analytical method, B-spline method, and piecewise linear method were employed. Since an analytical approach can simply describe tool surfaces with geometric primitives, this technique was first investigated. The analytical method combines lines, arcs, planes, cylinders and hemispheres to construct a whole tool surface. The B-spline technique is considered because of the numerical stability and computational efficiency. The B-spline method employs the cubic B-spline functions as its basis. A piecewise linear technique is adopted because it is relatively easy to construct and fast in computation. The piecewise linear method uses linear functions as its basis. In the B-spline and piecewise linear approaches to three-dimensional tool description, an array of equally-spaced points is required to find desired points quickly.

The raw tool surface data for fitting a continuous 3-D tool surface can be provided by various sources: a CAD/CAM system, digitizer, blueprint, analytical equation, etc., The raw data set is converted to a conditioned surface data set, i.e. equally-spaced data set for simple fitting to continuous representations for use in the FEM program.

5. NUMERICAL EXAMPLES

In order to examine the validity, accuracy and stability of 3-D FEM formulation and tool description methods, hemispherical and rounded square punch forming operations were simulated.

5.1 Hemispherical Punch

The chosen hemispherical punch test, Fig. 3, exhibits constant curvature, gentle radius, and a simple analytical representation. The axisymmetric specimen is initially flat and its material properties (corresponding to aluminum-killed 1008 steel sheet) are as follows (Knibloe, 1988):

Plastic anisotropy parameter: r=1.875,

Hill's non-quadratic yield function parameter: M=2,386,

Hardening law: $\bar{\sigma}=K(\bar{\varepsilon}+\dot{\varepsilon}_0)^n(\bar{\varepsilon}/\dot{\xi})^m$,

where $\bar{\sigma}$=effective stress $\bar{\varepsilon}$=effective strain

K=597.7(MPa) ε_0=0.0001

n=0.23 m=0.0129

$\dot{\xi}$=1.0(s^{-1}) $\dot{\bar{\varepsilon}}$=effective strain rate

Coulomb friction coefficient: μ=0.45

Thickness: t=1.0(mm)

Figure.4 represents the finite element mesh; it represents one

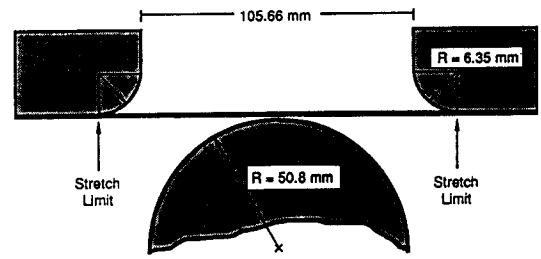

Fig. 3 Geometry of tooling for hemispherical punch forming operation

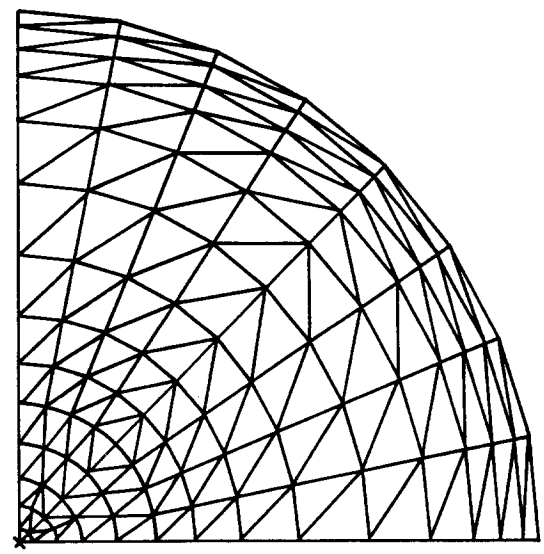

Fig. 4 Finite element mesh for simulating the hemispherical punch forming operation

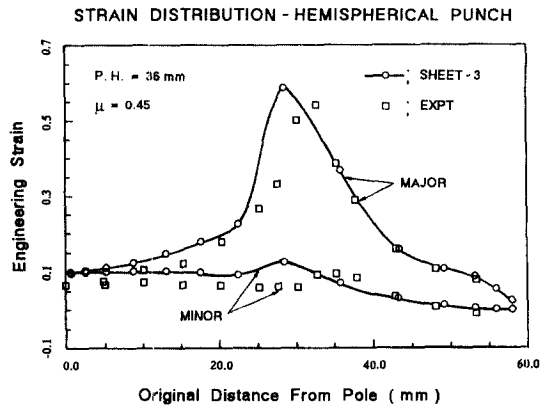

Fig. 5 Comparison of strain distributions between FEM (SHEET-3) and experiment(EXPT) (Knibloe) in the hemispherical punch forming operation

quarter of the physical blank. Perfectly-clamped (zero-displacement) boundary conditions are imposed at the outer perimeter and symmetric boundary conditions are specified along the radii. The number of nodes, elements and degrees of freedom employed in this analysis are 111, 184 and 288, respectively. The coefficient of friction used in the FEM analysis is chosen to fit best with previous experimental measurements(Knibloe, 1988).

Figure. 5 shows strain distributions along the original radial position at a punch height(P.H.) of 36mm in FEM analysis (SHEET-3) and experimental measurements(EXPT). The experimental strains shown in fig. 5 are middle-surface ones, which are calculated form the top and bottom strains in the average sense. Good agreements between FEM results and experimental measurements are found, except that peak points are shifted to the left.

3.2 Rounded Square Punch

The simulation of a square punch forming operation, whose punch surface has smaller and varying radii, was next performed. Figure. 6 shows the tooling geometry for the square punch forming operation, whose punch radius, R_p, is 9.53mm. Figure. 7 illustrates FEM mesh of one quarter of deformed area in the sheet blank. The number of nodes, elements and degrees of freedom employed in the simulation of stretch forming process are 290, 522 and 870, respectively. In the marked directions, "Normal" and "Diagonal" in Fig. 7, the FEM analyses are compared with experiments (Wnag and Wagoner, 1990).

The specimen is initially flat and its material properties (corresponding to aluminum-killed deep-drawing quality (AKSQ) steel) are as follows (Wang and Wagoner, 1990) :

Plastic anisotropy parameter : $r=1.75$,
Hill's non-quadratic yield function parameter : $M=2.0$,
Hardening law : $\bar{\sigma}=K(\bar{\varepsilon}+\varepsilon_0)^n(\dot{\bar{\varepsilon}}/\xi)^m$,
where $\bar{\sigma}$ =effective stress $\dot{\bar{\varepsilon}}$=effective strain
$K=563.5$(MPa) $\varepsilon_0=0.0001$
$n=0.227$ $m=0.0129$
$\xi=1.0(s^{-1})$ $\dot{\bar{\varepsilon}}$ =effective strain rate
Coulomb friction coefficient : $\mu=0.15$
Thickness : $t=1.0$(mm)

a perfectly-clamped (zero-displacement) boundary condition is imposed at the right-most perimeter and a symmetric boundary condition is specified at the left-most boundary or

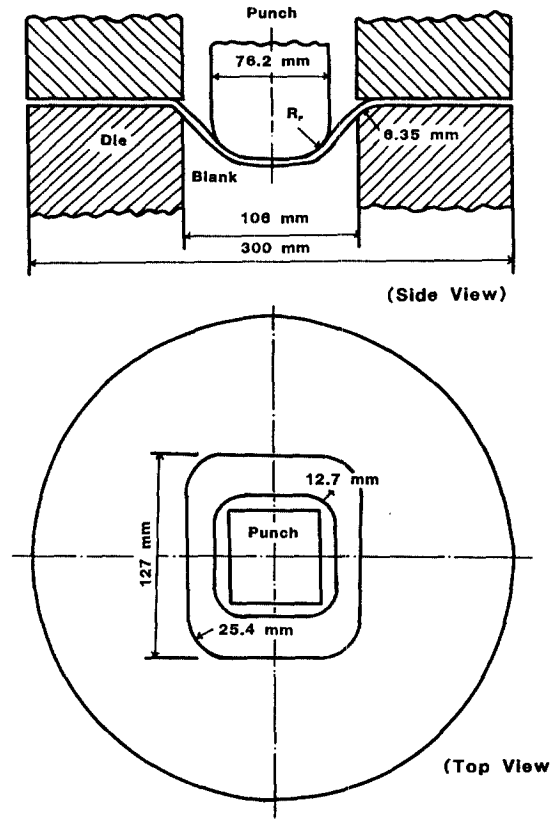

Fig. 6 Geometry of tooling for square punch forming operation.

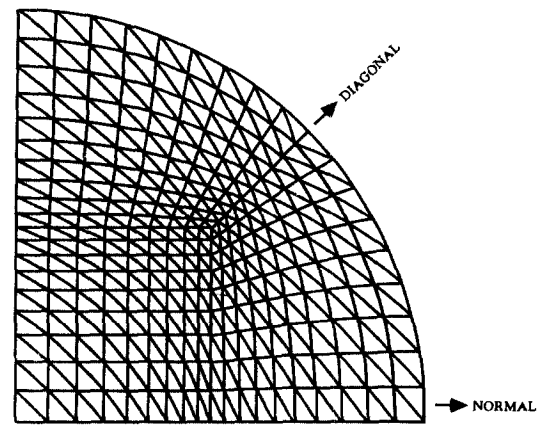

Fig. 7 Finite element mesh for simulating the square punch forming operation

specimen center. The friction coefficient was chosen to fit best with the experiment measurements.

Figure. 8(a) shows the comparison of strain distributions along the normal direction between the 3-D experiments (3-D Expt.) and 3-D FEM (SHEET-3) at the punch height (P.H.) of 11.4mm. A very good agreement appears except at the edge radii of the die, a discrepancy presumably introduced by ignoring bending in the simulation. Figure.8(b) compares strain distributions along the diagonal direction between 3-D FEM (SHEET-3) and full-size experiment (3-D Expt.) at the punch height (P.H.) of 11.5mm. Excellent agreement is found

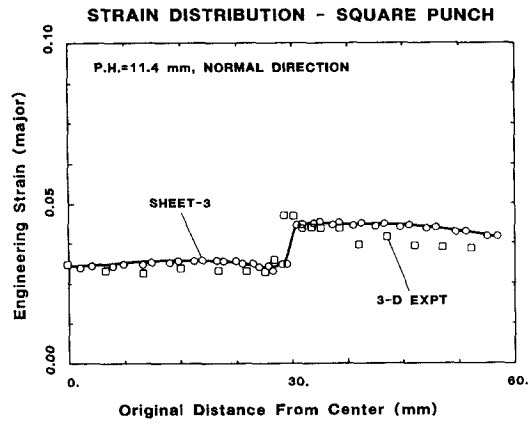

(a)

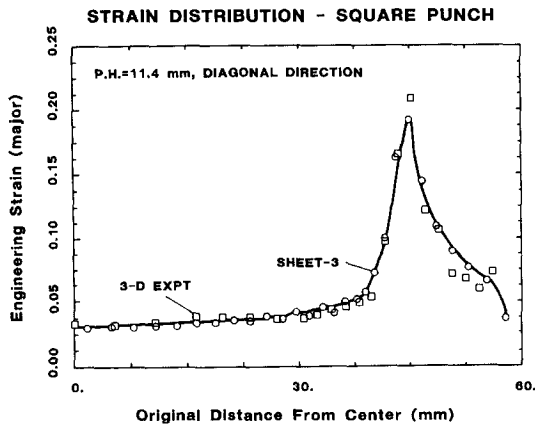

(b)

(a) along "Normal" and (b) along "Diagonal" directions in the square punch forming operation

Fig. 8 Comparison of strain distributions between FEM (SHEET-3) and experiment (3-D EXPT) (Wang and Wangoner)

between FEM results and experimental data. The 3-D FEM underestimates the peak strain, presumably a result of the fairly coarse mesh used. The simulation to a punch height of 15mm required about 6000 CPU seconds on a VAX-8550.

6. CONCLUSIONS

For the simulation of three-dimensional stretch sheet metal forming processes, an FEM program, SHEET-3, was developed. The mesh-based FEM/surface formulation which describes tool surfaces and FEM meshes compatibly and does not rely on spatial derivatives of the tool surface for evaluation of the friction and contact conditions was employed for the 3-D simulation of sheet metal stretch forming processes. In this formulation, the surface tangents, normals, and corresponding derivatives at each FEM node are directly evaluated from the FEM mesh, in terms of the connecting nodal positions.

In order to promote the convergence in Newton-Raphson iterations, the equilibrium and contact iterations are split. A quasi-linear scheme was also used for the indeterminacy of unloading.

The 3-D numerical examples for simple punch/die profiles verified the accuracy and efficiency of FEM formulation and illustrated the promise of success in the simulation of arbitrary-shaped real-world problems.

For the fast and accurate analysis of sheet forming operations, the following tasks are suggested: (1) Theoretical development and numerical implementation to include the bending effect are expected. (2) The numerical implementation of draw-in phenomena is necessary for the draw-die simulation. (3) A pre-processor, which automatically generates the tool data and mesh data from CAD/CAM system, should be developed to reduce the time in data preparation.

ACKNOWLEDGEMENTS

The authors first wish to thank Prof. J.K. Lee and Dr. E. Nakamachi for their discussions leading to these results. Also, thanks go to C.-T. Wang and J.R. Knibloe for providing experimental data for the comparison of FEM results. This work was supported by the Center for Net Shape Manufacturing at The Ohio State University, the Chrysler Corporation and the Ohio Supercomputer Center (PAS080).

REFERENCES

Bellet, M., Massoni,E. and Chenot,J.L., 1987, "A Viscoplastic Membrane Formulation for the 3-Dimensional Analysis of Thin Sheet Metal Forming," Proc. Int. Conf. on Comp. Plas., Barcelona, Spain, Pineridge Press, pp.917~986.

Chung,S.Y. and Swift, S.W., 1951, "Cup Drawing from a Flat Blank: Part I -Experimental Investigation; Part II-Analytical Investigation," Proc. Inst. Mech. Eng., pp.165~199.

Damamme,G., 1978, "Minimum de la Deformation Generalisee d'un Element de Matiere, Pour les Chemins de Deformation Passant d'un Etat Final Donne," Comlptes Rendus Acad. Sc. Paris, 287a, p.895.

Drucker, D.C., 1951, "A More Fundamental Approach to Plastic Stress-Strain Relations," Proc. 1st U.S. Nat'l Congress of Appl. Mech., ASME.

Germain,Y., Chung,K. and Wagoner, R.H., 1989, "A Rigid Visco-Plastic Finite Element Program for Sheet Metal Forming Analysis," Int. J. Mech. Sci., Vol.31, No.1, pp.1~24.

Hill,R., 1979, "Theoretical Plasticity of Textured Aggregates," Math. Proc. Camb. Phil.Soc., Vol.85, pp.179~191.

Keum,Y.T., Nakamachi,E., Wagoner,R.H. and Lee,J.K., 1990, "Compatible Description of Tool Surfaces and FEM Meshes for Analyzing Sheet Forming Operations," Int. J. Num. Meth. Eng., Vol.30, pp.1471~1502.

Keum,Y.T., 1990, Compatible Description of Tool Surfaces and FEM Meshes for Analyzing Sheet Forming Operations in Two-and Three-Dimensions, Ph.D. Dissertation, The Ohio StateUniversity.

Knibloe,J.R., 1988, Experimental Investigation and Finite Element Modeling of Hemispherically Stretched Steel Sheet, M.S.Thesis, The Ohio State University.

Kobayashi,S. and Kim,J.H., 1978, "Deformation Analysis of Axisymmetric Sheet Metal Forming Processes by the Rigid-plastic Finite Element Method." Mechanics of sheet Metal Forming, D.P Koistinen and N.M. Wang eds., Plenum Press, New-York, pp.341~363.

Massoni,E., Bellet,M., Abouaf,M. and Chenot,J.L., 1986,

"Large Displacements Numerical Calculation of 3-Dimensional Elasto-Plastic and Elasto-Viscoplastic Membrane by the Finite Element Method," Numerical Methods for Non-Linear Problems, Pineridge Press, Vol.3, pp.480~493.

Mellor,P.B. and Parmer,A., 1978, "Plasticity Analysis of Sheet Metal Forming," Mechanics of Sheet Metal Forming, D.P. Koistinen and N.M. Wang eds., GMR, Warren, Michigan, Plenum Press, N.Y., pp.53~77.

Oh,S.I. and Kobayashi,S., 1980, "Finite Element Analysis of Plane Strain Sheet Bending," Int. J. Mech. Sci., Vol.22, pp.583~594.

Onate,E. and Zienkiewicz, O.C., 1978, "Plastic Flow of Axisymmetric Thin Shells as a Non-Newtonian Flow Problem and its Application to Stretch Forming and Deep Drawing Problems," Proc. of IDDRG 10th Biennial Congress, Warwick, England, Portcullis Press Ltd., Reedfill, Surrey, U. K..

Onate,E. and Zienkiewicz, O.C., 1983, "A Viscous Formulation for the Analysis of Thin Sheet Metal Forming," Int. J. Mech. Sci., Vol.25, No.5, pp.305~335.

Park,J.J., Oh,S.I. and Altan,T., 1987, "Analyses of Axisymmetric Sheet Forming Processes by Rigid-Viscoplastic Finite Element Method," J. Eng. Ind., ASME Trans., Vol.109, pp.347~354.

Tang,S.C., 1976, "Elasto-plastic and Large Deformation Analysis of Thin Sheels by the Deformation Theory of Plasticity," Comp. Structures, Vol.6, pp.297~303.

Toh,C.H. and Kobayashi,S., 1983, "Finite Element Process Modelling of Sheet Metal Forming of General Shapes," Proc. International Symposium on Fundamentals of Metal Forming Technique-State and Trends, Stuttgart, Germany, pp.39~56.

Wang,N.-M., 1976, "A Mathematical Model of Sheet Metal Forming Operations," MA-104, General Motors Research Laboratories, Warren, MI, U.S.A..

Wang,N.-M. and Wenner,M.L., 1978, "Elastic-Viscoplastic Analysis of Simple Stretch Forming Problems," Mechanics of Sheet Metal Forming, D.P. Koistinen and N.M. Wang eds., GMR, Warren, Mi, Plenum Press, N.Y., pp.367~391.

Wang,N.-M., 1982, "A Rigid-Plastic Rate-Sensitive Finite Element Procedure for Sheet Metal Forming Calculations." Numerical Methods in Industrial Forming Processes, J.F.T. Pittsman, R.D. Wood, J.M. Alexander and O.C. Zienkiewicz eds., Pineridge Press, Swansea, U.D. pp.797~806.

Wang,N.-M., 1982, A Rigid-Plastic Rate-Sensitive Finite Element Mehtod for Modeling Sheet Metal In-plane Stretching, GMR-4079, General Motors Research Laboratory, Warren, MI, U.S.A..

Wang,N.-M., 1984, "A Rigid-Plastic Rate-Sensitive Finite Element Method for Modeling Sheet Metal Forming Processes," Proc. Numerical Analysis of Forming Processes, J.F.T. Pittsman et al. eds., John Wiley & Sons, pp.117~164.

Wang,G.-T. and Wagoner,R.H., 1990, "Square-Punch Forming: Experiments and Simulations in 2-D and 3-D," *J.* Mech. Working Technol., Accepted for publication.

Wood,R.D., Mattiasson,K., Honner,M.E. and Zienkiewicz, O.C., 1978, "Viscous Flow and Sold Mechanics Approaches to the Analysis of Thin Sheet Forming," Computer Modelling of Sheet Metal Forming Process, N.M. Wang and S.C. Tang eds., The Metallurgical Society, Warrendale, PA, U.S.A., pp. 121~142.

Yang,D.Y., Chung,W.J. and Shim,H.B., 1990, "Rigid-Plastic Finite Element Analysis of Sheet Metal Forming Processes with Initial Guess Generation," Int. J. Mech. Sci., Vol.32, pp. 687~708.